European Journal of Pharmaceutics and Biopharmaceutics 132 (2018) 192–199

Contents lists available at ScienceDirect

European Journal of Pharmaceutics and Biopharmaceutics

journal homepage: www.elsevier.com/locate/ejpb

Research paper

In vitro and *in vivo* comparison between crystalline and co-amorphous salts of naproxen-arginine

Georgia Kasten[a], Lonita Lobo[b], Swapnil Dengale[b], Holger Grohganz[a], Thomas Rades[a], Korbinian Löbmann[a,*]

[a] Department of Pharmacy, University of Copenhagen, Universitetsparken 2, Copenhagen, Denmark
[b] Manipal College of Pharmaceutical Sciences, Manipal Academy of Higher Education, Madhava Nagar, India

ARTICLE INFO

Keywords:
Co-amorphous formulations
Amino acid
Salts
Dissolution
In vivo
Oral bioavailability study

ABSTRACT

Liquid-assisted grinding (LAG) and dry ball milling (DBM) have recently been used to obtain different physical forms of drug-amino acid salts with promising dissolution and physical stability properties. In this work, crystalline and co-amorphous naproxen-arginine mixtures were prepared using LAG and DBM, respectively, and compared with regard to their *in vitro* and *in vivo* performance. X-ray powder diffraction and Fourier-transformed infrared spectroscopy showed that LAG led to the formation of a crystalline salt, while DBM led to a co-amorphous salt. These results agreed with the differential scanning calorimetry profiles: a melting point of 230 °C was determined for the crystalline salt, while the co-amorphous formulation showed a single glass transition temperature at approx. 92 °C. Both solid state forms of the salt showed increased intrinsic dissolution rates (14.8 and 74.1-fold, respectively) and also higher solubility (25.3 and 29.8-fold, respectively) compared to the pure crystalline drug *in vitro*. Subsequently, the co-amorphous salt revealed an improved bioavailability in a pharmacokinetic study, showing a 1.5-fold increase in $AUC_{0\text{-}t}$ and a 2.15-fold increase in c_{max} compared to the pure crystalline drug. In contrast, even though showing a better *in vitro* performance, the crystalline salt interestingly did not show an increase in bioavailability in comparison to pure crystalline naproxen.

1. Introduction

Salt formation is the most widely used technique in the industry to improve solubility and dissolution rate of poorly water-soluble drugs [1–3]. Basically, crystalline salts are multicomponent crystals containing anionic and cationic atoms or molecules in a stoichiometric ratio. It is generally accepted that a salt between an acid-base pair can be obtained when their pK_a difference is greater than 2 [4].

Another technique to enhance solubility and dissolution rate is amorphization. In the amorphous form, there is no three-dimensional long-range order to be disrupted upon dissolution, and combined with its higher internal energy and reactivity, the drug potentially has a higher apparent solubility, and hence, higher rates of absorption [5,6]. A recent formulation approach to stabilize the inherently unstable amorphous form of a drug is co-amorphization, where a given drug is combined with a second low molecular weight component to form a homogenous amorphous phase [7]. This approach was employed to stabilize the amorphous form of several poorly water-soluble drugs, including *inter alia* indomethacin [8,9], furosemide [10], simvastatin [11,12], carbamazepine [9], and cimetidine [13].

Recently, the co-amorphous formulation technique has been combined with salt formation, especially between acidic drugs and basic amino acids [14–17]. In a previous study, Kasten and co-workers (2017) have shown that different solid state forms of indomethacin-lysine salts could be obtained by varying ball milling techniques [17]. When a solvent drop was added, in a liquid-assisted grinding process, the product formed was a crystalline salt. However, when a simple dry ball milling process was employed, the product formed was a co-amorphous salt. The authors reported on the influence of the physical form of such salts on the dissolution of the drug. The intrinsic dissolution rate of the crystalline salt was 32.7-fold higher compared to pure crystalline indomethacin, while the co-amorphous salt had a 90-fold higher intrinsic dissolution rate. Co-amorphization thus further enhanced the dissolution rate of indomethacin by 2.8 times compared to the crystalline salt. Due to the strong intermolecular interactions, the co-amorphous salt remained amorphous for at least 36 weeks under dry conditions. Similarly, highly stable co-amorphous systems have been reported in other studies when strong ionic interactions between the drug and the co-former were present [15,18,19].

Naproxen (NAP) is a non-steroidal anti-inflammatory drug (NSAID)

* Corresponding author.
E-mail address: korbinian.loebmann@sund.ku.dk (K. Löbmann).

https://doi.org/10.1016/j.ejpb.2018.09.024
Received 22 May 2018; Received in revised form 5 September 2018; Accepted 24 September 2018
Available online 25 September 2018
0939-6411/

used in the treatment of common ailments such as fever, headache and pain [20,21] by the inhibition of the cyclooxygenase enzyme [22]. Chemically, the drug is a chiral molecule having acidic properties with a pKa around 4.15 [23], and belongs to class II (low solubility, high permeability) of the Biopharmaceutics Classification System [24]. Crystalline salts of the *S* and *R* enantiomers of NAP with the basic amino acid arginine (ARG) produced by solvent evaporation can be found in the literature [25]. In addition, a co-amorphous salt between NAP and ARG has also been reported [15], however, the two physical forms (crystalline *vs* co-amorphous) of this salt have not been compared to each other yet.

In this study, we performed a comparative investigation of the crystalline and the co-amorphous salts between NAP and ARG *in vitro* and *in vivo*. For this purpose, 'liquid-assisted grinding' (LAG) and 'dry ball milling' (DBM) were used as preparation methods. The solid state properties of the two different NAP-ARG salts were investigated by X-ray powder diffraction, differential scanning calorimetry, thermogravimetric analysis and Fourier-transformed infrared spectroscopy. Furthermore, physical stability and *in vitro* performance (intrinsic dissolution and supersaturation ability) were investigated. Finally, a rat pharmacokinetic study was performed to assess the translation between the *in vitro* performance and *in vivo* response. Despite the recent interest in co-amorphous formulations, little on their *in vivo* performance is known. In fact, to the authors' knowledge, this is the first study to investigate the potential of crystalline and co-amorphous drug-AA salts *in vivo*.

2. Materials and methods

2.1. Materials

The acidic drug (*S*)-naproxen (NAP, Form I, M_w = 230.26 g/mol, pK_a = 4.15) was purchased from Divis Laboratories Ltd. (Florham Park, NJ, USA) and the basic amino acid L-arginine (ARG, M_w = 174.2 g/mol, pK_a = 9.0 and 12.48) was purchased from Sigma Aldrich (St. Louis, MO, USA). Potassium dihydrogen phosphate was also purchased from Sigma-Aldrich, and di-sodium hydrogen phosphate heptahydrate was kindly donated by Merck (Darmstadt, Germany). All substances were of reagent grade and used as received. Their chemical structures are shown in Fig. 1.

2.2. Methods

2.2.1. Preparation of NAP-ARG salts

Liquid-assisted grinding (LAG) was employed to obtain the crystalline salt between NAP and ARG. Briefly, 1.0 g of the powder containing NAP and ARG at an equimolar ratio was transferred to 25 mL milling jars containing two stainless steel balls of 12 mm diameter each, with the addition of 50 µL of ultrapure water. The ball mill (Mixer mill MM400, Retsch GmbH & Co., Haan, Germany) was set at 30 Hz and placed in a cold room (6 °C). The milling lasted 60 min and the product was collected for further analysis. After the milling, the solvent was allowed to evaporate overnight over P_2O_5 in a desiccator before further analyses. For the preparation of the co-amorphous salt, a similar milling process was used, however, no solvent was added, resulting in a dry ball milling (DBM) experiment. For comparison, 1.0 g of pure NAP and pure ARG were milled, using the same LAG and DBM conditions described above.

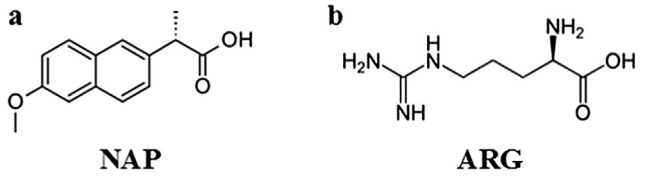

Fig. 1. Chemical structures of (a) NAP and (b) ARG.

In addition, the kinetics of formation of a crystalline salt (or co-amorphization) were studied at different times of milling. After an initial physical mixing of the compounds for 5 min in the ball mill but without the stainless steel balls, the latter were added. Thereafter, the milling process was stopped at predetermined times (1, 5, 15, 30 and 60 min) and approx. 10 mg of powder was collected and analyzed by XRPD.

2.2.2. X-ray powder diffraction (XRPD)

XRPD analysis was performed on an ẊPert PRO X-ray diffractometer (PANalytical, Almelo, The Netherlands) with Cu Kα radiation (1.5418 Å), and an acceleration voltage and current of 45 kV and 40 mA, respectively. The samples were scanned in reflectance mode between 5 and 35° 2θ, with a scan rate of 0.0625° 2θ/s and a step size of 0.026° 2θ. The data was collected and analyzed using the software packages X'Pert Data Collector and X'Pert Highscore Plus (PANalytical, Almelo, The Netherlands).

Furthermore, the experimentally obtained diffractogram for the crystalline NAP-ARG salt was compared to the crystalline structures of NAP-ARG salts deposited in the Cambridge Structure Database (reference codes JASHOB and QANPEB). The respective powder diffractograms were calculated using the Mercury v3.9 software (CCDC, Cambridge, England).

2.2.3. Thermal analysis

Differential scanning calorimetry (DSC) measurements were performed using a DSC Discovery (TA Instruments, New Castle, USA) under a nitrogen flow of 50 mL/min. Powder samples of approx. 1–6 mg were weighed into Tzero aluminum pans and closed with Tzero lids. The crystalline salt, physical mixtures and crystalline pure components were analyzed by DSC in standard temperature mode, with a heating rate of 10 °C/min, from 25 to 240 °C. The melting points (T_m) were recorded as the peak onset temperatures of three replicates using Trios v3.3.0.4055 software (TA Instruments-Waters LLC, New Castle, USA). Thermal analysis of the co-amorphous salt was conducted in the modulated temperature mode, with a heating rate of 2 °C/min (amplitude of 0.212 °C and period of 40 s) from -10 °C to 180 °C. The experimental glass transition temperatures (T_g, midpoint) were recorded in the reversing heat flow signal of three replicates using Trios software.

Thermogravimetric analysis (TGA) was employed to assess the presence of solvent residue and thermal degradation. Approx. 10 mg of powder was added to platinum pans in a TGA Discovery (TA Instruments, New Castle, USA), which were heated from 25 to 300 °C at a heating rate of 10 °C/min, under a nitrogen flow of 50 mL/min. Weight loss (in percentage) was determined using Trios software.

2.2.4. Fourier-transformed infrared spectroscopy (FTIR)

FTIR analysis was performed on an MB3000 instrument (ABB Inc, Quebec, Canada), coupled to an attenuated total reflectance accessory with a ZnSe plate (MIRacle Single Reflection ATR, PIKE Technologies, Fitchburg, USA). The infrared spectra of pure NAP and ARG and the NAP-ARG salts were collected between 4000 and 600 cm^{-1}, and calculated as a mean of 32 spectra with a resolution of 4 cm^{-1} using New Horizon MB software (ABB Inc, Quebec, Canada).

2.2.5. Physical stability studies upon storage

For storage studies, dry conditions (relative humidity ~ 2%) were obtained in a desiccator at 25 °C using P_2O_5, and at 40 °C using silica gel. Humid conditions (relative humidity ~ 75%) at 25 °C were obtained using a saturated sodium chloride solution. The humidity levels were continuously monitored by EasyLog EL-USB2 sensors (Lascar Electronics, Essex, England). The recrystallization tendency was then investigated by XRPD 1, 2, 4, 8, 20, 36 and 48 weeks after sample preparation.

2.2.6. Intrinsic dissolution rate (IDR)

The IDR was determined under sink conditions. For this, 150 mg of powder samples were compressed inside stainless steel cylinders by a hydraulic press Model IXB-102-9 (Perkin Elmer, Ueberlingen, Germany) set at 125 MPa for 10 s, resulting in a disc with an area of 0.7854 cm^2. The cylinders containing the samples were placed in 900 mL of 10 mM phosphate buffer (pH 6.8, 37 °C) and stirred at 50 rpm. Aliquots of 5 mL were withdrawn at predetermined time points (0.5, 1, 3, 5, 10 and 15 min) and immediately replaced with fresh dissolution media. All intrinsic dissolution experiments were conducted in triplicate.

HPLC analysis of the dissolution samples was conducted using a Dionex liquid chromatographer equipped with an UltiMate 3000 pump and UltiMate 3000 detector (Thermo Scientific, MA, USA). The mobile phase consisted of a mixture of methanol and 10 mM phosphate buffer pH 6.8 at a 1:1 ratio (v/v), with flow of 0.8 mL/min. A Kinetex C18 (100 mm × 4.6 mm, 5 μm) column (Phenomenex Inc., California, USA) was used. The injected volume was 15 μL. The retention time of NAP was 2.47 min, while each run lasted 5 min. The same standard curve (0.1–20 μg/mL, $R^2 = 0.999$) was used both for both, NAP and NAP-ARG samples, at a detection wavelength of 271 nm, as ARG did not interfere with the UV absorption of NAP at this wavelength.

The IDR was calculated as described previously by Löbmann et al. [13] determining the slope of the regression line for the release-time profile of NAP per accessible area ($mg \cdot cm^{-2}$).

2.2.7. Powder dissolution

Powder dissolution and supersaturation ability were investigated under non-sink conditions for 24 h. Briefly, a scaled-down USP2 apparatus consisting of a set of mini glass vessels with rotating mini paddles (Erweka DT 70, Heusenstamm, Germany) was used [26]. A volume of 150 mL of 10 mM phosphate buffer (pH 6.8, 37 °C) was used as medium and the rotation speed was set to 100 rpm. 5.0g of powder was added to each vessel and 1 mL samples were collected at 2, 5, 10, 20, 30, 60, 120, 240, 360, 720 and 1440 min of dissolution and immediately replaced with fresh phosphate buffer. The samples were centrifuged in a Heraeus Megafuge 16R (Thermo Fisher Scientific Inc., Waltham, MA, USA) for 7 min at 10.000 rpm, and quantified by UV spectrophotometry at 271 nm (2.5–100 μg/mL, $R^2 = 0.9994$). All experiments were performed in triplicate.

2.2.8. Oral bioavailability studies

In vivo oral bioavailability studies were approved by the animal ethics committee (IAEC) of Manipal University (protocol number IAEC/KMC/47/2016). Male albino Wistar rats of 200 g ± 20 g were employed for the pharmacokinetic studies in a parallel design, with 6 rats in each group. The rats were fasted overnight with free access to water for at least 12 h. A dose equivalent of 5.0 mg/kg of NAP was suspended in 25 mM phosphate-buffered carboxymethyl cellulose (pH 6.8) and administered orally by gavage to three groups of rats: group 1 received crystalline naproxen (NAP), group 2 the crystalline salt (crystalline NAP-ARG) and group 3 the co-amorphous salt (co-amorphous NAP-ARG). The administered total volume was 1.0 mL. At predetermined time points (0.25, 0.5, 1, 1.5, 2, 3, 5, 8 and 12 h) after drug administration, approx. 0.15 mL of blood was collected by retro-orbital bleeding under diethyl ether anesthesia, transferred into heparinized tubes and centrifuged at 10,000 rpm for 10 min in a Remi cooling centrifuge (Model C-24, Mumbai, India). The plasma was separated into clean tubes and frozen at −70 °C until further analysis.

Plasma analysis was performed on an Alliance Waters 2695 HPLC (Waters Corporation, Milford, USA) and UV dual lambda absorbance detector (Waters 2487). A Grace smart C18 (250 × 4.6 mm ID × 5 μm) column and a mobile phase constituting of a mixture of acetonitrile and phosphate buffer (25 mM, pH 3.2) in a 45:55 (v/v) ratio were used. The eluent was monitored at 230 nm at a flow rate of 1.0 mL/min, with indomethacin (IND) being the internal standard (IS). The auto-sampler and column oven temperature were maintained at 4 °C and 25 °C, respectively. The injection volume was 20 μL and the retention times of NAP and IND (IS) were 5.89 and 9.88 min, respectively. The method was validated as per FDA Bioanalytical methods validation [27] over a calibration range of 2.5–50 μg/mL, and the quality control samples were distributed amongst the calibration and pharmacokinetic samples. Specificity and selectivity of the method were assessed in the presence of ARG to rule out the possibility of any interference with the retention times of either drug or IS.

For the sample preparation, 10 μL of IS (IND 200 μg/mL) was added to 50 μL of plasma standard or sample followed by 50 μL of phosphate buffer (100 mM, pH 3.2) and vortexed for 15 s. Subsequently, 1.6 mL of tertiary butyl methyl ether was added to the samples, vortexed for 5 min, and then subjected to centrifugation at 10,000 rpm at 4 °C (Remi centrifuge Model C-24, Mumbai, India). The supernatant was then separated and evaporated under a stream of nitrogen at 40 °C for 15 min and reconstituted with 500 μL of mobile phase. Finally, the sample was transferred to a total recovery vial, and 20 μL was injected into the HPLC system.

The calculation of pharmacokinetic parameters was made by using a non-compartmental model and PK solutions 2.0 software (Summit research solutions, Montrose, CO, USA). An ANOVA followed by Tukey's *post-hoc* test was used to determine any significant differences between the controls and formulations ($p < 0.05$) with Minitab version 17 software (Minitab Inc., State College, PA, USA).

3. Results and discussion

3.1. Solid state characterization

The solid state properties of pure NAP and pure ARG, physical mixture and milled formulations were assessed by XRPD and DSC, in order to investigate potential differences in the physical forms of the products obtained during salification between the acidic drug NAP and the basic amino acid ARG.

Upon LAG and DBM, the individual compounds, NAP and ARG remained crystalline and did not change their respective crystalline form compared to the crystalline starting materials (data not shown). When milled in combination, however, the NAP-ARG mixture turned into a crystalline formulation by LAG, and into a co-amorphous formulation by DBM after 60 min of milling. The crystallization and co-amorphization kinetics are visualized for LAG and DBM in Fig. 2a-b, respectively.

The physical mixture presented high crystallinity with sharp reflections at '0 min'. Upon LAG, a reduction in crystallinity at '1 min' and '5 min' of milling was initially observed followed by a nearly amorphous sample at '15 min'. Subsequently, the intensity of the diffractions increased upon further milling as seen in the diffractograms after '30 min' and '60 min' of milling (Fig. 2a), with the appearance of new crystalline reflections not present in the starting material (the physical mixture at '0 min'). In contrast, when DBM was applied the initial physical mixture was transformed gradually into an amorphous form as indicated by the amorphous halo formation after '60 min' of milling (Fig. 2b).

Investigating the crystalline salt further, new reflections were formed in the LAG product (as indicated by the red dotted lines in Fig. 3a), e.g. at 6.0°, 19.7° and 26.6° 2θ, while the black dotted lines represent reflections corresponding to the initial materials, e.g. at 12.6° and 17.9° 2θ from NAP and 23.1° 2θ from ARG. It is also important to notice the disappearance of important reflections in the new LAG product, such as the reflections at 6.6° for NAP and 27.4° 2θ for ARG. Salts of (S)-Nap-(S)-Arg and (R)-Nap-(S)-Arg were previously obtained by solvent evaporation [25], and their crystallographic information is reported in the Cambridge Structural Database (CSD) as 'JASHOB' and 'QANPEB', respectively. Hence, the powder X-ray diffraction patterns of these NAP-ARG salts were calculated with Mercury 3.9 software,

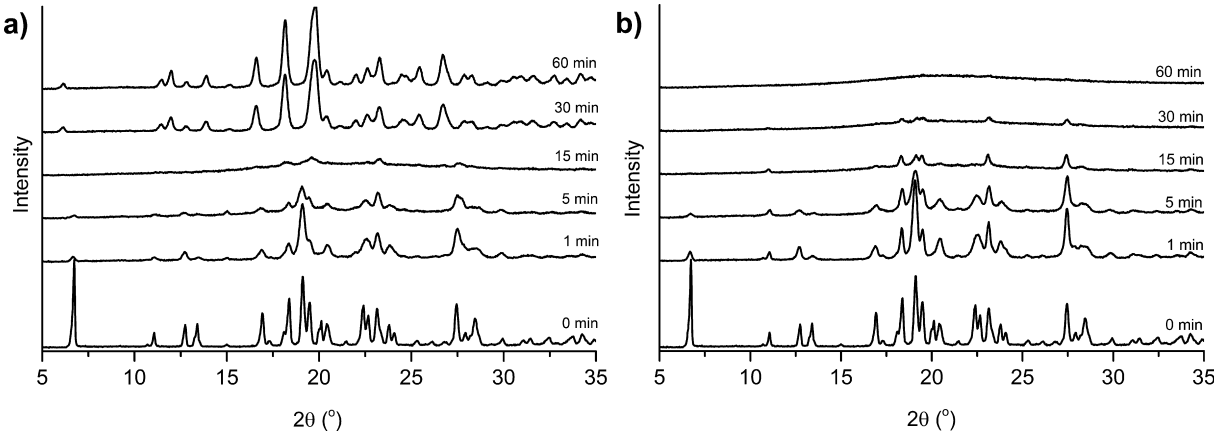

Fig. 2. XRPD diffractograms of NAP-ARG formulations, showing (a) changes in the crystalline reflections during LAG with increasing milling time, and (b) an amorphous halo formation for DBM after 60 min of milling.

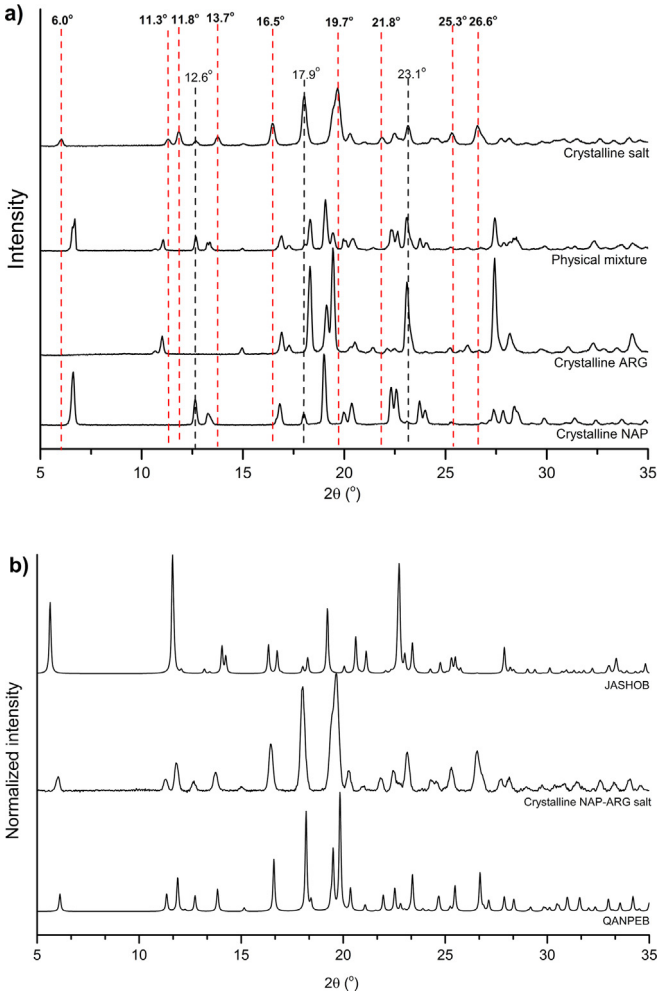

Fig. 3. (a) XRPD peak analysis for the crystalline NAP-ARG salt product compared to the initial components and a physical mixture between NAP and ARG; (b) XRPD peak analysis between the CSD salt structures for (S)-Nap(S)-Arg ('JASHOB') and (R)-Nap(S)-Arg ('QANPEB'), compared to the crystalline NAP-ARG salt obtained by LAG.

normalized, and compared to the crystalline LAG product obtained in this study (Fig. 3b). The calculated QANPEB diffractogram is very similar to the one obtained by LAG, suggesting that indeed a crystalline salt between NAP and ARG was obtained. Interestingly, a chiral inversion of (S)-NAP to (R)-NAP occurred during LAG, since (S)-NAP was used as starting material however, a (R)-NAP-(S)-ARG salt was obtained. It has previously been reported that such an inversion may occur with NAP during *in vivo* drug metabolization [41] or during water treatment [42,43]. It appears that the presence of the chiral molecule ARG and water during LAG could have unintentionally induced the inversion in stereochemistry of NAP. Chiral inversion has also been seen for other "profen" molecules, such as ibuprofen and ketoprofen, and this phenomenon requires further investigation.

The formation kinetics of the crystalline NAP-ARG salt (Fig. 2a) are furthermore in line with reported findings on the formation of a crystalline salt *via* an amorphous intermediate step during milling, recently described for the acid-base pair indomethacin-lysine by Kasten et al. [17]. Here, the authors discussed that the disorder and increased molecular mobility that occurred during initial amorphization lead to a crystalline salt product in the presence of water, given that the intensity of the new reflections increased until the end of the milling experiment. This indicated an enhanced kinetics of crystalline salt formation in the presence of a solvent, a process that seems to apply also to the NAP-ARG crystalline salt obtained in this work.

To further investigate the solid state of the milled products, thermal analysis (DSC) was used. To investigate the formation of a crystalline salt upon LAG, the crystalline starting materials are compared to the crystalline LAG product (Table 1). The melting event of NAP (T_m = 155.4 °C) indicated that the drug is initially present as NAP form I [28]. Pure ARG presented a melting event at 215.3 °C followed by thermal degradation. In contrast, the LAG product showed that a new melting point (T_m = 230.4 °C) that was substantially higher than the melting points of pure NAP and ARG, suggesting that indeed a new solid form was created between NAP and ARG. Interestingly, Vayá and coworkers [25] reported that both (R)-Nap(S)-Arg and (S)-Nap(S)-Arg salts obtained by solvent evaporation exhibited melting points between 188 and 201 °C and 189–202 °C with degradation, differing substantially from the T_m of 230.4 °C measured in this work.

Furthermore, modulated temperature DSC analysis of the co-amorphous salt showed that a homogenous co-amorphous product was indeed obtained by DBM, as a single T_g was observed [29–30] at 91.9

Table 1
Melting points of the crystalline starting materials and crystalline NAP-ARG prepared by LAG.

Sample	Preparation technique	Melting point onset (± SD) (°C)
NAP	Starting material	155.4 (± 0.0)
ARG	Starting material	215.3 (± 0.1)*
NAP-ARG LAG	LAG	230.4 (± 0.0)*

* Degradation is observed upon melting as indicated by TGA.

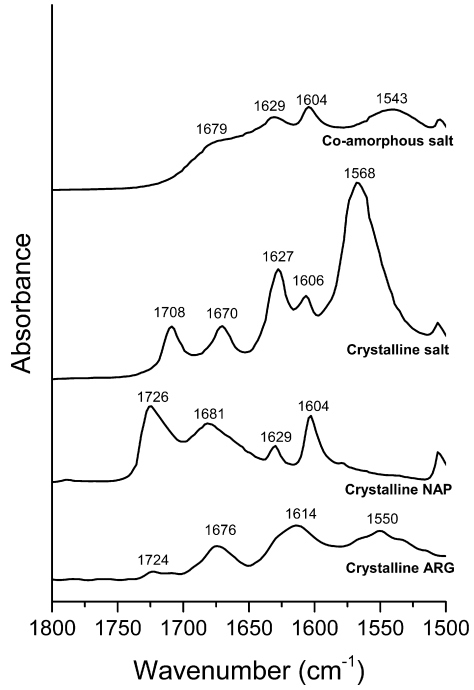

Fig. 4. FTIR spectra of crystalline ARG and NAP, crystalline and co-amorphous NAP-ARG salts obtained by LAG and DBM, respectively.

(± 0.2) °C.

3.2. Molecular interactions

FTIR was used to confirm the observed salt formation after the LAG and DBM processes. Generally, the symmetric stretch relative to the free carboxylic acid group of a given drug is found between 1700 and 1725 cm^{-1} and the antisymmetric stretch of the corresponding ionized carboxyl group between 1505 and 1610 cm^{-1} [11,15,16]. Thus, the spectral region between 1800 and 1500 cm^{-1} was selected for analysis (Fig. 4).

The FTIR spectra of the LAG and DBM products were compared to those of the crystalline drug and AA used, since their pure amorphous forms could not be obtained by milling or quench cooling. It is commonly known that peak broadening and/or peak shifts can occur when comparing crystalline and the respective amorphous form of solids, due to altered molecular arrangement and near range order in the amorphous form [31], and in that sense, careful considerations should be made when comparing the spectra of pure crystalline NAP and ARG to the spectra of LAG and DBM formulations.

Crystalline NAP is an acidic drug and its free carboxylic acid symmetric stretch can be seen at 1726 cm^{-1}. After milling in combination with ARG, the carboxyl group ionized and the respective vibration appeared as a new broad peak with high intensity at 1568 cm^{-1} for the crystalline formulation, and with lower intensity at 1543 cm^{-1} for the co-amorphous formulation. Furthermore, the crystalline salt shows the vibration of the ARG carbonyl band at 1708 cm^{-1} [32], which is less pronounced and part of the broad shoulder at 1679 cm^{-1} in the spectrum of the co-amorphous salt. Overall, the DBM and LAG spectra are similar, even though the intensity of the bands of the crystalline salt are more pronounced, while the bands of the co-amorphous salt are overlapped and less intense. Hence, together with the XRPD analysis, thermal behavior, and literature findings, a successful salt formation between NAP-ARG upon DBM and LAG is suggested.

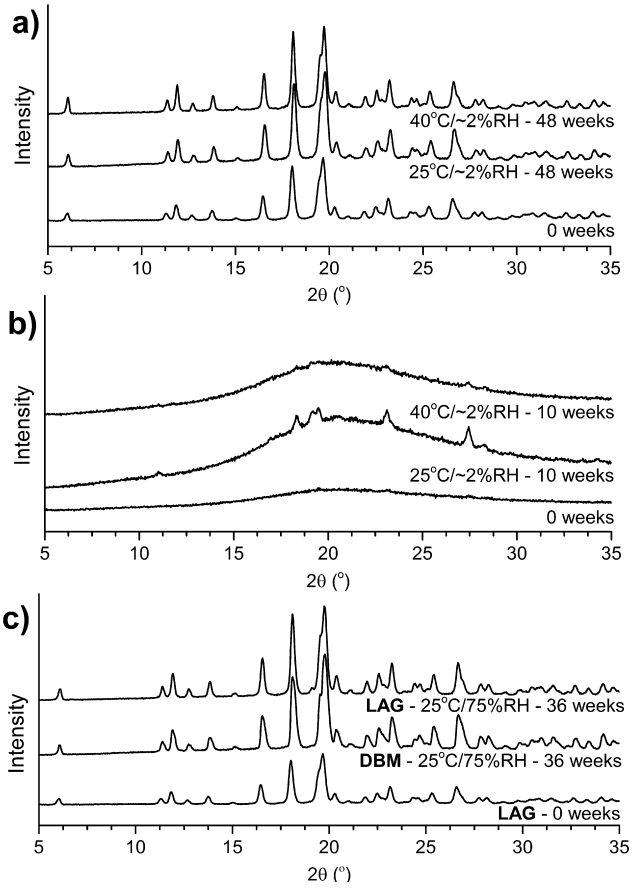

Fig. 5. Diffractograms of NAP-ARG salt formulations upon storage. (a) Crystalline salts obtained by LAG after 0 and 48 weeks of storage at 25 and 40 °C, dry conditions; (b) co-amorphous salts obtained by DBM after 0 and 10 weeks of storage at 25 and 40 °C, dry conditions; (c) transition of co-amorphous salt obtained by DBM to crystalline salt (similar to the one obtained by LAG) when stored at 25 °C, humid conditions.

3.3. Physical stability

The physical stability study aimed to investigate the tendency of different formulations to recrystallize or show polymorphic transitions when stored at different temperatures (25 and 40 °C) and relative humidity (RH) conditions (~2 and 75% RH).

Under dry conditions, the crystalline salt remained in the same crystalline form (Fig. 5a) whilst the co-amorphous salt presented small recrystallization peaks after 10 weeks, at both temperatures (Fig. 5b). The reflections observed at 11.0°, 18.3°, 19.1°, 19.6°, 23.1°, and 27.4° 2θ indicate that the component beginning to recrystallize is the amino acid ARG, suggesting that the co-amorphous salt did undergo a phase separation into its individual components.

However, under high humidity (75% RH, 25 °C) the storage of co-amorphous DBM samples led to recrystallization within 10 days (in Fig. 5c the diffractogram after 36 weeks of storage in shown due to higher intensity of crystalline reflections). The co-amorphous salt recrystallized into the crystalline salt since its diffractogram became similar to that of the LAG crystalline samples. This finding supports the fact that the addition of water in the LAG process can induce a (crystalline) salt formation, and it is in line with the findings previously reported for co-amorphous and crystalline indomethacin-lysine salts [17].

3.4. Dissolution studies

The intrinsic dissolution rate (IDR) of the formulations was

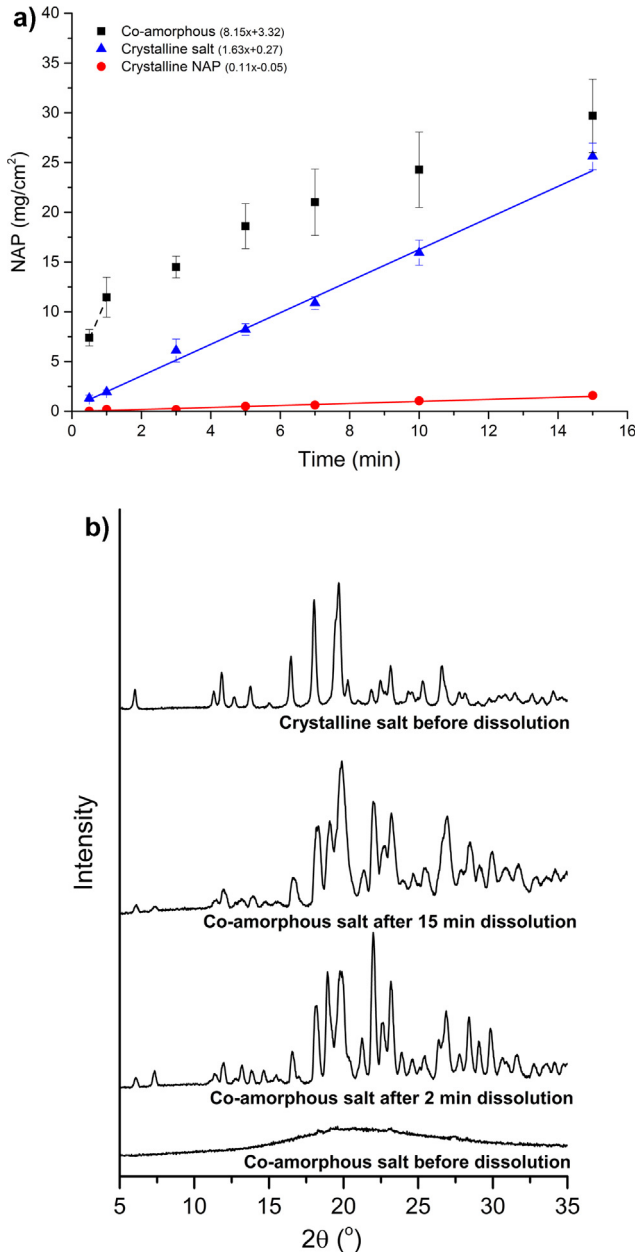

Fig. 6. (a) Intrinsic dissolution profiles of crystalline NAP, and crystalline and co-amorphous salts of NAP-ARG; (b) XRPD of co-amorphous formulations before and after 2 and 15 min of IDR test, and of the crystalline salt before dissolution.

determined for the first minutes of dissolution in pH 6.8 buffered solution and used to study the influence of the physical form on the dissolution of the salts obtained by LAG and DBM, *i.e.* crystalline versus co-amorphous salts of NAP-ARG, respectively. The curves and dissolution rates are shown in Fig. 6a.

Pure crystalline NAP presented a slow dissolution rate (0.11 ± 0.01 mg·cm^{-2}·min^{-1}) whereas the crystalline salt formulation showed a considerably higher dissolution rate (1.63 ± 0.15 mg·cm^{-2}·min^{-1}, 14.8-fold higher than for crystalline NAP). The dissolution profile of the co-amorphous salt is considerably higher than the dissolution of the crystalline salt in the first two minutes (8.15 ± 3.32 mg·cm^{-2}·min^{-1}), but a change in slope occurred thereafter due to a fast recrystallization upon contact with the aqueous dissolution medium [33–35], as shown by the diffractograms of the compact's surface layer after starting the IDR test (Fig. 6b). The obtained

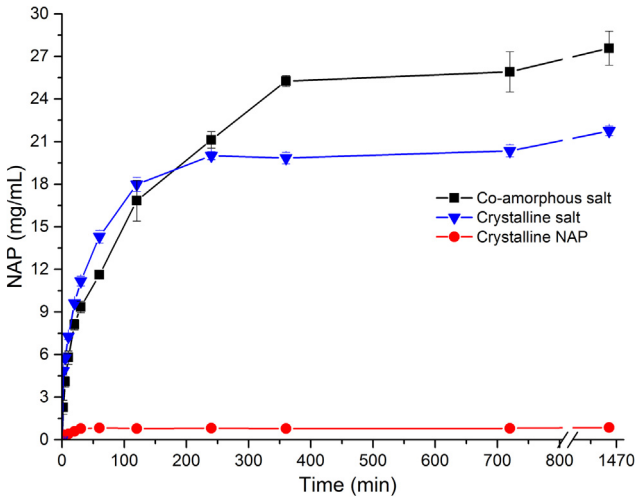

Fig. 7. Powder dissolution of pure crystalline NAP, and NAP-ARG crystalline and co-amorphous salts.

diffractogram showed reflections for both, the crystalline salt and pure NAP, suggesting that the initially co-amorphous salt converted to a mixture of these two crystalline materials.

In order to study the supersaturation ability given by the fast dissolution rate inherent to amorphous and co-amorphous formulations [36], non-sink powder dissolution tests were carried out for 24 h. A comparison between pure crystalline NAP and the crystalline and co-amorphous NAP-ARG salts is shown in Fig. 7. Pure crystalline NAP exhibited a slow increase in concentration in the first minutes of dissolution and reached a plateau from 60 min until 24 h, with a maximum concentration (c_{max}) of 0.86 ± 0.01 mg/mL of drug dissolved. Salt formation, on the other hand, promoted a significant increase in dissolution, as already seen during IDR above. The crystalline salt formulation showed a 25.3-fold increase in c_{max}, reaching 21.75 ± 0.33 mg/mL of NAP dissolved, exhibiting a fast spring effect in the first 60 min of dissolution, and then reaching a plateau after 120 min that extended until the end of the experiment. This probably reflects the saturation solubility of the crystalline salt in these conditions. The co-amorphous salt provided an even higher c_{max}, of 25.58 ± 1.20 mg/mL, this concentration being 29.8-fold higher than that of pure crystalline NAP and 1.2-fold higher than its crystalline salt counterpart, supporting the hypothesis that both salt formation and co-amorphization can contribute to improved dissolution and solubility of poorly aqueous soluble drugs, as both samples contained similar amounts of ARG. Further, no significant deviations in pH were observed. Interestingly, in the light of the fast solid state conversation (< 2 min) observed in the previous IDR experiment, higher concentrations of NAP were reached after 240 min from the co-amorphous salt compared to the crystalline salt. In addition, the (low degree of) supersaturation reached by the co-amorphous salt after 360 min was maintained until the end of the experiment (24 h), which may be beneficial for achieving an improved bioavailability [36–38].

XRPD was performed on the excess solid phase by the end of the powder dissolution tests. For pure NAP the initial crystalline polymorph (NAP Form I) was found, and for the crystalline salt its undissolved LAG salt form was found (data not shown). The initially co-amorphous salt, however, was encountered as a mixture of crystalline NAP and the LAG salt, which is in line with the previous experiments that demonstrated the effect of water on the conversion of the co-amorphous salt to the crystalline salt.

The dissolution results point out the great importance of the physical form of drug-AA salt forms: co-amorphization is crucial for the extent of dissolution and supersaturation achieved during the *in vitro* dissolution tests, resulting in the most pronounced increase for the co-

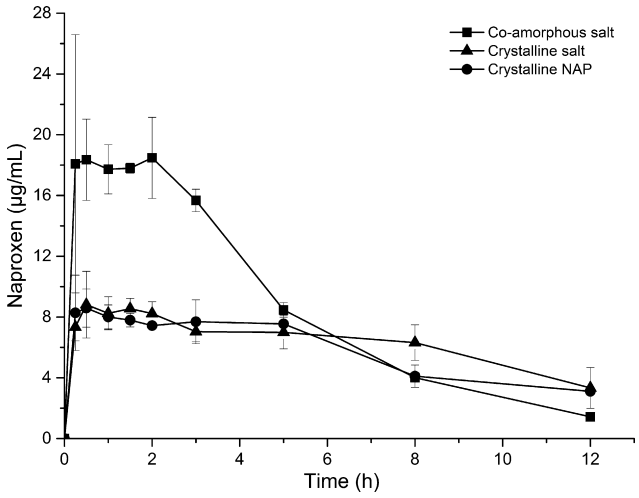

Fig. 8. Mean plasma concentration–time profile for crystalline NAP, crystalline salt and co-amorphous salt.

Table 2
Pharmacokinetic parameters after single oral dose equivalent to 5 mg/kg of NAP for pure crystalline NAP, crystalline salt and co-amorphous salt (n = 6).

Parameter	Crystalline NAP	Crystalline salt	Co-amorphous salt
c_{max} (µg/mL)	8.59 (± 1.25)	8.82 (± 2.20)	18.48 (± 2.67)*
t_{max} (h)	0.5	0.5	2.0
$t_{½}$ (h)	9.95	4.34	2.70
$AUC_{(0-t)}$ (µg·h/mL)	69.68 (± 13.27)	76.54 (± 9.74)	104.62 (± 11.86)*
V_d (mL)	1029.71	817.79	186.09

* $p < 0.05$ significantly different.

amorphous NAP-ARG salt compared to its crystalline salt and pure crystalline NAP.

3.5. Oral bioavailability profile

To investigate whether the *in vitro* dissolution advantage of the crystalline and co-amorphous salts also translates into an *in vivo* oral bioavailability advantage, pharmacokinetic studies were performed on Wistar rats. The comparative pharmacokinetic profiles of crystalline NAP, crystalline salt and co-amorphous salt formulations are shown in Fig. 8 and Table 2.

Overall, NAP appears to be rapidly absorbed from all formulations. The maximum plasma concentration (c_{max} of 8.59 ± 1.25 µg/mL) of crystalline NAP was achieved after 0.5 h (t_{max}), which is in line with other pharmacokinetic studies on crystalline NAP [20,39,40]. Furthermore, the crystalline salt presented a similar c_{max} and $AUC_{(0-t)}$ compared to pure NAP (Fig. 8). Hence, the improved solubility and dissolution rate of the crystalline salt *in vitro* was not reflected in an improved bioavailability *in vivo*. An explanation for this finding is that the ionized form of NAP from the LAG salt transformed into the unionized species of NAP in the acidic environment of the stomach of the rats (data not shown), therefore, showing a similar plasma-concentration profile as pure NAP.

On the other hand, the improved dissolution properties of the co-amorphous salt shown *in vitro*, e.g. the faster initial dissolution in the IDR experiments and the supersaturation achieved during powder dissolution, were also reflected *in vivo*. The higher bioavailability was reflected in a higher c_{max} of 18.48 ± 2.67 µg/mL, $AUC_{(0-t)}$ of 104.62 ± 11.86 µg·h/mL, and an also extended t_{max} of 2.0 h (Table 2). Therefore, the co-amorphous salt showed a significant increase of approx. 1.5-fold in AUC_{0-t} and 2.15-fold in c_{max} compared to pure NAP (or the crystalline NAP-ARG salt). Despite the possibility of precipitation of NAP in the acidic environment of the stomach, interestingly, it appears that the solubility and dissolution advantage of the co-amorphous salt formulation was translated into the *in vivo* experiment.

4. Conclusions

In this work, crystalline and co-amorphous drug-amino acid salts were prepared by LAG or DBM, respectively, and their performance was further investigated *in vitro* and *in vivo*. The XRPD, DSC and FTIR analyses indicated the crystalline nature of the LAG formulation as well as the formation of the co-amorphous salt upon DBM. Physical stability studies showed that the crystalline salt was physically stable during the 48 weeks storage period assessed under dry and humid conditions. In contrast, the co-amorphous salt showed recrystallization of ARG after 10 weeks under dry conditions (25 and 40 °C), however, under humid conditions (25 °C) a crystallization into the crystalline salt already after 10 days was observed. The crystalline salt presented a faster dissolution rate when compared to crystalline NAP, but the largest advantage was shown by the co-amorphous salt, which presented a fast initial IDR (< 2 min) and also a supersaturation ability *in vitro*. Interestingly, the high solubility and dissolution of the crystalline salt were not translated into an enhanced *in vivo* pharmacokinetic profile. On the other hand, the co-amorphous salt exhibited a significantly higher *in vivo* bioavailability when compared to pure NAP and crystalline salt.

5. Declarations of interest

None.

Acknowledgements

GK would like to thank Conselho Nacional de Desenvolvimento Científico e Tecnológico (CNPq) of the Ministry of Science, Technology and Innovation of Brazil (203432/2014-2) for the financial support, and also Christoffer Gerner Bavnhøj Hansen and Rikke Dueholm for the support on 24 h dissolution studies.

References

[1] A.T.M. Serajuddin, Salt formation to improve drug solubility, Adv. Drug Deliv. Rev. 59 (2007) 603–616.
[2] K.T. Savjani, A.K. Gajjar, J.K. Savjani, Drug solubility: importance and enhancement techniques, ISRN Pharm. 195727 (2012) 1–10.
[3] D.P. Elder, R. Holm, H.L. Diego, Use of pharmaceutical salts and cocrystals to address the issue of poor solubility, Int. J. Pharm. 453 (2013) 88–100.
[4] P.H. Stahl, C.G. Wermuth (Eds.). Handbook of Pharmaceutical Salts: Properties, Selection, and Use. VHCA, Verlag Helvetica Chimica Acta, Zürich, Switzerland, and Wiley-VCH, Weinheim, Germany, 2002.
[5] B.C. Hancock, G. Zografi, Characteristics and significance of the amorphous state in pharmaceutical systems, J. Pharm. Sci. 86 (1) (1997) 1–12.
[6] A. Beyer, L. Radi, H. Grohganz, K. Löbmann, T. Rades, C.S. Leopold, Preparation and recrystallization behavior of spray-dried co-amorphous naproxen–indomethacin, Eur. J. Pharm. Biopharm. 104 (2016) 72–81.
[7] S.J. Dengale, H. Grohganz, T. Rades, K. Lobmann, Recent advances in co-amorphous drug formulations, Adv. Drug Deliv. Rev. 100 (2016) 116–125.
[8] N. Chieng, J. Aaltonen, D. Saville, T. Rades, Physical characterization and stability of amorphous indomethacin and ranitidine hydrochloride binary systems prepared by mechanical activation, Eur. J. Pharm. Biopharm. 71 (2009) 47–54.
[9] K. Löbmann, H. Grohganz, R. Laitinen, C. Strachan, T. Rades, Amino acids as co-amorphous stabilizers for poorly water soluble drugs – Part 1: Preparation, stability and dissolution enhancement, Eur. J. Pharm. Biopharm. 85 (2013) 87–881.
[10] K.T. Jensen, F.H. Larsen, C. Cornett, K. Löbmann, H. Grohganz, T. Rades, Formation mechanism of coamorphous drug–amino acid mixtures, Mol. Pharm. 12 (7) (2015) 2484–2492.
[11] K. Löbmann, C. Strachan, H. Grohganz, T. Rades, O. Korhonen, R. Laitinen, Co-amorphous simvastatin and glipizide combinations show improved physical stability without evidence of intermolecular interactions, Eur. J. Pharm. Biopharm. 81 (1) (2012) 159–169.
[12] R. Laitinen, K. Löbmann, H. Grohganz, C. Strachan, T. Rades, Amino acids as co-amorphous excipients for simvastatin and glibenclamide: physical properties and stability, Mol. Pharm. 11 (2014) 2381–2389.
[13] S. Yamamura, H. Gotoh, Y. Sakamoto, Y. Momose, Physicochemical properties of amorphous salt of cimetidine and diflunisal system, Int. J. Pharm. 241 (2002) 213–221.
[14] K.T. Jensen, L.I. Blaabjerg, E. Lenz, A. Bohr, H. Grohganz, P. Kleinebudde, T. Rades,

K. Löbmann, Preparation and characterization of spray-dried co-amorphous drug-amino acid salts, J. Pharm. Pharmacol. 68 (2016) 615–624.
[15] K.T. Jensen, K. Löbmann, T. Rades, H. Grohganz, Improving co-amorphous drug formulations by the addition of the highly water soluble amino acid, proline, Pharmaceutics 6 (2014) 416–435.
[16] Y. Huang, Q. Zhang, J.-R. Wang, K.-L. Lin, X. Mei, Amino acids as co-amorphous excipients for tackling the poor aqueous solubility of valsartan, Pharm. Dev. Technol. 22 (1) (2017) 69–76.
[17] G. Kasten, K. Nouri, H. Grohganz, T. Rades, K. Löbmann, Performance comparison between crystalline and co-amorphous salts of indomethacin-lysine, Int. J. Pharm. 533 (2017) 138–144.
[18] M. Allesø, N. Chieng, S. Rehder, J. Rantanen, T. Rades, J. Aaltonen, Enhanced dissolution rate and synchronized release of drugs in binary systems through formulation: amorphous naproxen–cimetidine mixtures prepared by mechanical activation, J. Control. Release 136 (2009) 45–53.
[19] W. Wu, K. Löbmann, T. Rades, H. Grohganz, On the role of salt formation and structural similarity of co-formers in co-amorphous drug delivery systems, Int J Pharm. 535 (2018) 86–94.
[20] H.B. Hucker, A.G. Zacchei, S.V. Cox, D.A. Brodie, N.H.R. Cantwell, Studies on the absorption, distribution and excretion of indomethacin in various species, J. Pharm. Exp. Ther. 153 (2) (1966) 237–249.
[21] P.N.P. Rao, E.E. Knaus, Evolution of nonsteroidal anti-inflammatory drugs [NSAIDs]: cyclooxygenase (COX) inhibition and beyond, J. Pharm. Pharmaceut. Sci. 11 (2) (2008) 81s–110s.
[22] H. Sevelius, R. Runkel, E. Segre, S.S. Bloomfield, Bioavailability of naproxen sodium and its relationship to clinical analgesic effects, Br. J. Clin. Pharmac. 10 (1980) 259–263.
[23] G.L. Amidon, H. Lennernas, V.P. Shah, J.R. Crison, A theoretical basis for a biopharmaceutic drug classification: the correlation of in vitro drug product dissolution and in vivo bioavailability, Pharm. Res. 12 (1995) 413–420.
[24] I. Vayá, M.C. Jiménez, M.A. Miranda, Stereodifferentiation in the fluorescence of naproxen-arginine salts in the solid state, Tetrahedron: Assymmetry 16 (2005) 2167–2171.
[25] S. Moyer, Pharmacokinetics of naproxen sodium, Cephalalgia 6 (4) (1986) 77–80.
[26] S. Klein, V.P. Shah, A standardized mini paddle apparatus as an alternative to the standard paddle, AAPS Pharm. Sci. Tech. 9 (4) (2008) 1179–1184.
[27] FDA Draft Guidance for Industry, Bioanalytical methods validation, Food and Drug Administration, Rockville, MD, 2013.
[28] J.-S. Song, Y.-T. Sohn, Crystal forms of naproxen, Arch. Pharm. Res. 34 (1) (2011) 87–90.
[29] W.L. Chiou, S. Riegelman, Pharmaceutical applications of solid dispersion systems, J. Pharm. Sci. 60 (9) (1971) 1281–1302.
[30] J.A. Baird, L.S. Taylor, Evaluation of amorphous solid dispersion properties using thermal analysis techniques, Adv. Drug Deliv. Rev. 64 (2012) 396–421.
[31] A. Heinz, C.J. Strachan, K.C. Gordon, T. Rades, Analysis of solid-state transformations of pharmaceutical compounds using vibrational spectroscopy, J. Pharm. Pharmacol. 61 (2009) 971–988.
[32] M.W. Forbes, M.F. Bush, N.C. Polfer, J. Oomens, R.C. Dunbar, E.R. Williams, R.A. Jockusch, Infrared spectroscopy of arginine cation complexes: direct observation of gas-phase zwitterions, J. Phys. Chem. A 111 (46) (2007) 11759–11770.
[33] B.C. Hancock, M. Parks, What is the true solubility advantage for amorphous pharmaceuticals? Pharm. Res. 17 (4) (2000) 397–404.
[34] D.E. Alonzo, G.G.Z. Zhang, D. Zhou, Y. Gao, L.S. Taylor, Understanding the behavior of amorphous pharmaceutical systems during dissolution, Pharm. Res. 27 (4) (2010) 608–618.
[35] N. Fotaki, C.M. Long, K. Tang, H. Chokshi, Dissolution of amorphous solid dispersions: theory and practice, in: N.H. Shah, H.K. Sandhu, D.S. Choi, H.K. Chokshi, W. Malick (Eds.), Amorphous Solid Dispersions, Springer, New York, USA, 2014.
[36] J. Brouwers, M.E. Brewster, P. Augustijns, Supersaturating drug delivery systems: the answer to solubility-limited oral bioavailability? J. Pharm. Sci. 98 (8) (2009) 2549–2572.
[37] J. Chen, L.-I. Mosquera-Giraldo, J.D. Ormes, J.D. Higgins, L.S. Taylor, Bile salts as crystallization inhibitors of supersaturated solutions of poorly water-soluble compounds, Cryst. Growth Des. 15 (2015) 2593–2597.
[38] M. Yang, W. Gong, Y. Wang, L. Shan, Y. Li, C. Gao, Bioavailability improvement strategies for poorly water-soluble drugs based on the supersaturation mechanism: an update, J. Pharm. Pharm. Sci. 19 (2) (2016) 208–225.
[39] T.B. Vree, M. Van Den Biggelaar-Martea, C.P. Verwey-Van Wissen, M.L. Vree, P.J. Guelen, The pharmacokinetics of naproxen, its metabolite O-desmethylnaproxen, and their acyl glucuronides in humans. Effect of cimetidine, Br. J. Clin. Pharmacol. 35 (5) (1993) 467–472.
[40] P.W. Elsinghorst, M. Kinzig, M. Rodamer, U. Holzgrabe, F. Sörgel, An LC–MS/MS procedure for the quantification of naproxen in human plasma: development, validation, comparison with other methods, and application to a pharmacokinetic study, J. Chromatog. B 879 (19) (2011) 1686–1696.
[41] H. Ikuta, A. Kawase, M. Iwaki, Stereoselective pharmacokinetics of ibuprofen in inflammation, Drug Metab. Dispos. 45 (3) (2017) 316–324.
[42] T. Suzuki, Y. Kosugi, M. Hosaka, T. Nishimura, D. Nakae, Occurrence and behavior of the chiral anti-inflammatory drug naproxen in an aquatic environment, Environ. Toxicol. Chem. 33 (12) (2014) 2671–2678.
[43] D. Camacho-Muñoz, B. Petrie, E. Castrignanò, B. Kasprzyk-Hordern, Enantiomeric profiling of chiral pharmacologically active compounds in the environment with the usage of chiral liquid chromatography coupled with tandem mass spectrometry, Curr. Anal. Chem. 12 (4) (2016) 303–314.